Unusual Features of the Membrane Kinome of *Trypanosoma brucei*

Bryan C. Jensen[a]*, Pashmi Vaney[b%], John Flaspohler[c], Isabelle Coppens[d], and Marilyn Parsons[a,e]

[a]Center for Global Infectious Disease Research, Seattle Children's Research Institute, 307 Westlake Ave. N., Seattle, WA 98109

[b]Seattle Biomedical Research Institute, 307 Westlake Ave. N, Seattle, WA 98109#

[c]Biology Department, Concordia College, 901 8th St. S, Moorhead, MN 56562

[d]Department of Molecular Microbiology and Immunology, Johns Hopkins School of Public Health, 615N. Wolfe Street, Baltimore, MD 21205

[e]Departments of Pediatrics and Global Health, University of Washington, Seattle, WA, 98195

% current address: Adaptive Biotechnologies, 1551 Eastlake Ave E, Suite 200. Seattle WA, 98102

*corresponding author

#Seattle Biomedical Research Institute merged with Seattle Children's Research Institute in 2018

Abstract

In many eukaryotes, multiple protein kinases are situated in the plasma membrane where they respond to extracellular ligands. Ligand binding elicits a signal that is transmitted across the membrane, leading to activation of the cytosolic kinase domain. Humans have over 100 receptor protein kinases. In contrast, our search of the *Trypanosoma brucei* kinome showed that there were only ten protein kinases with predicted transmembrane domains, and unlike other eukaryotic transmembrane kinases, seven are predicted to bear multiple transmembrane domains. Most of the ten kinases, including their transmembrane domains, are conserved in both *Trypanosoma cruzi* and *Leishmania* species. Several possess accessory domains, such as Kelch, nucleotide cyclase, and forkhead-associated domains. Surprisingly, two contain multiple regions with predicted structural similarity to domains in bacterial signaling proteins. A few of the protein kinases have previously been localized to subcellular structures such as endosomes or lipid bodies. We examine here the localization of epitope-tagged versions of seven of the predicted transmembrane kinases in *T. brucei* bloodstream forms and show that five localized to the endoplasmic reticulum. The last two kinases are integral membrane proteins associated with the flagellum, flagellar pocket, or adjacent structures, as shown by both fluorescence and immunoelectron microscopy. Thus, these kinases are positioned in structures suggesting participation in signal transduction from the external environment.

Introduction

With its complex life cycle spanning different hosts and tissues, the response of *Trypanosoma brucei* to its environment is a subject of considerable interest. In other eukaryotes, signaling by extracellular molecules is initiated by ligand binding, typically to proteins situated at the plasma membrane. The most prominent categories of such proteins are G-protein coupled receptors (absent in trypanosomatids) and protein kinases (PKs) [1]. *T. brucei* also possesses a large family of surface proteins that have external ligand-binding domains and internal adenylate cyclase domains [2], although the ligands and signaling pathways involved remain to be elucidated. Transporters can also function in signal transduction by internalizing regulatory molecules such as Pi or cGMP [3-5]. In *T. brucei*, a plasma membrane carboxylate transporter is important in regulating the transition of mammalian bloodstream forms (BF) to the insect procyclic form (PF) stage [6].

Eukaryotes tend to have hundreds of PKs that bear the signature eukaryotic PK (ePK) motifs in the catalytic domain, *T. brucei* has ~180 protein-coding regions that bear a canonical ePK domain [7]. Almost all PK orthologues are shared among *T. brucei*, *Trypanosoma cruzi* and *Leishmania major*. Most eukaryotes have tens to hundreds of PKs that bear transmembrane domains (TMDs), and in metazoans almost all are tyrosine kinases that reside in the plasma membrane. Ligand binding to the extracellular

domain generates a signal that is transduced to the cytosolic catalytic domain resulting in kinase activation. In a previous analysis of the genome, we identified ten PKs predicted to bear TMDs as predicted by TMHMM [7], The redrawing of CDS boundaries based on 5' transcript mapping eliminated the putative TMD of one (Tb927.10.16160) and annotation of another PK was updated to include a TMD (Tb927.10.1910). The catalytic domains of these PKs cluster with serine/threonine kinases [7].

About half of the *T. brucei* TMD PKs have been characterized functionally. Tb927.2.2720, dubbed *MEKK1* (so-named for the similarity of its catalytic domain to MAP kinase kinase kinases), is required for the quorum sensing pathway that triggers proliferating slender BF to enter stationary phase as a prelude to transmission [8]. Tb927.11.14070, known as *RDK1*, encodes a repressor of BF to PF differentiation [9]. Tb927.11.8940 encodes LDK (lipid droplet kinase), which is present on lipid droplets and essential for their biogenesis [10]. Tb927.4.2500, which encodes an eIF2 kinase-related protein, EIF2K2K, is localized to the flagellar pocket [11]. While the function of this kinase in *T. brucei* is not known, its orthologue in *Leishmania* appears to regulate promastigote to amastigote development [12] and the *T. cruzi* orthologue similarly regulates the development of infective epimastigote forms [13]. Tb927.10.1910 is suggested to play a role in melarsoprol sensitivity on the basis of high-throughput RNAi assays [14]. Cell death was not observed upon depletion of the TM kinases in BF in a kinome-wide stem-loop RNAi study, although the degree of knockdown was not quantitated [9].

Here we report studies examining the TMD PKs. Many of them have unusual domain structures, such as the presence of multiple TMDs, nucleotide cyclase domains, or regions of structural similarity to bacterial signaling modules. We examined the subcellular localization of seven of these PKs in monomorphic BF, which are unable to differentiate to PF. Five of the tagged PKs localized predominantly to the endoplasmic reticulum (ER), indicating they entered the secretory system. Two were found to have particularly distinctive distributions: FHK localized to a region at or near the flagellar pocket and MEKK1 localized similarly, as well as the flagellum. Immunoelectron microscopy of cultured PF confirmed the unique positioning of these two kinases.

Results

Domain structure. Figure 1A depicts schematics of the ten *T. brucei* PKs that have TMDs, showing the location of the TMDs. Also shown are the PK catalytic domains and additional domains listed on TriTrypDB (based primarily on sequence similarities), plus regions HHpred identified as having predicted structural similarities to other protein modules. These PKs are large, with the smallest (the lipid droplet kinase LDK) being 553 aa, about twice the size of the PK domain, and the rest ranging from 929 to 1678 aa. The PK domain of all of these kinases, with the exception of LDK, resides at the C-terminus.

81 Transmembrane domains and signal peptides. Surprisingly, seven of the ten proteins are predicted by
82 TMHMM to be multi-pass proteins, having two or more TMDs, a topology that is extremely uncommon
83 for eukaryotic PKs. We therefore re-examined the TMD (predicted by TMHMM and shown TriTrypDB,
84 red bars in Fig. 1) using CCTOP (Constrained Consensus TOPology Prediction,
85 http://cctop.enzim.ttk.mta.hu/, which combines ten algorithms with structural data to yield a model. The
86 CCTOP models concurred with TMHMM for four PKs and proposed additional TMDs for the rest of the
87 PKs (Fig. 1, red arrowheads), and rejected one of the TMDs on RDK1 (red x). Some of the additional
88 TMDs predicted with CCTOP are unlikely to be authentic since they occur in the middle of domains, for
89 example, one that punctuates the ePK catalytic domain in Tb927.5.3150, and those within structural
90 domains of RDK1 and Tb927.9.3120. When we examined the orthologues of these *T. brucei* PKs in *L.*
91 *major* and *T. cruzi*, the number and position of the TMHMM-predicted TMDs generally concurred (Table
92 S1). The exceptions included the *L. major* orthologue of eIF2K2 (LmjF.34.2150), the *T. cruzi* CL-Brener
93 orthologues of Tb927.5.3150, and the *T. cruzi* orthologue of LDK (TcCLB.511801.14), all of which lack
94 a TMHMM-predicted TMD. However, CCTOP did predict TMDs in these proteins. Furthermore, since
95 LDK resides in a monolayer membrane surrounding lipid droplets rather than a bilayer, algorithms may
96 be less proficient at identifying relevant membrane insertion/association sequences. While it is not
97 possible to be certain of the number of TMDs from bioinformatic predictions, an even number of TMDs
98 would place the N- terminal region and C-terminal catalytic domain in the same compartment. For
99 example, MEKK1 is predicted to have a hairpin of two TMDs, separated by only four aa. The extended
100 N- and C-regions would either both be cytosolic, or both be extracellular. We are unaware of any
101 transmembrane kinases that display catalytic domains on the external face of the plasma membrane, so
102 propose that the former possibility is most likely.

103 Most membrane proteins destined for the secretory system or plasma membrane enter the ER membrane
104 co-translationally, courtesy of a signal peptide or a transmembrane domain [15]. Interestingly, it has been
105 proposed that two TMDs separated by loop, such as seen in MEKK1 and several other TMD kinases (Fig.
106 1), may be a topogenic signal for insertion into the ER membrane [16]. Two of the PKs bearing TMDs are
107 also predicted to bear signal peptides: eIF2K2 and Tb927.5.3150. Three additional *T. brucei* PKs are
108 annotated as bearing signal peptides, but they lack predicted TMDs.

109 Domains identified by sequence similarity. Searches based on sequence similarity showed that
110 Tb927.5.3150 bears two Kelch/Kelch-like domains, which often participate in protein-protein
111 interactions. Additional domains related to signaling functions were detected on several PKs. Three bear
112 nucleotide cyclase-like domains (Tb927.3.5650, Tb927.9.12400, and Tb927.10.1910). Interestingly these
113 are the only *T. brucei* PKs identified as having such domains, although the parasite genome encodes

114 multiple adenylyl cyclases with cytoplasmic catalytic domains and presumed ligand-binding extracellular
115 domains [17]. One PK (Tb927.9.3120) contains a region related to PAS (Per-Arnt-Sim) domains, which
116 usually function to bind small molecules or proteins intracellularly. Forkhead kinase, FHK,
117 Tb927.7.5220) is so-named for the presence of a forkhead-associated domain; these domains typically
118 interact with phosphopeptides (usually phosphothreonine in specific contexts) [18].

119 Conserved folds identified by structural predictions. The PKs were also subjected to HHpred analysis to
120 identify regions with predicted structural similarity to protein structures available in the protein database
121 PDB [19] (Fig. 1). The domains mentioned above all showed numerous matches with the related domains
122 on other proteins, with probability scores of over 99%. A PAS-like region on FHK was additionally
123 identified by HHpred, with multiple hits having a probability above 90%.

124 Surprisingly, two PKs have large regions of predicted structural similarity to molecular signaling modules
125 present in bacteria. RDK1 includes two regions with predicted structural similarity to other signaling
126 molecules (Fig. S1). The first is similar to bacterial sensor/receptor domains, such the ligand binding
127 domain of *Pseudomonas aeruginosa* histamine receptor TlpQ [20] and the extracellular domains of a set
128 of bacterial histidine kinases for which the ligands are unknown [21]. This region is followed by a
129 predicted TMD and then a segment predicted to fold similarly to full-length catalytic domains of several
130 bacterial and eukaryotic adenylyl/guanylyl cyclases. The cyclase region is followed by the eukaryotic PK
131 catalytic domain. This organization suggests that the sensor-like domain lies on the opposite side of the
132 membrane to the cyclase and PK domains. The modular organization of RDK1 is conserved in other
133 trypanosomatids, as well as the more distantly related free-living bodonid *Bodo saltans* [22].

134 Tb927.9.3120 has co-linear regions predicted to fold similarly to molecules involved in bacterial
135 signaling: histidine kinases and response regulators. The histidine kinases typically contain sensing
136 modules, followed by DHp dimerization regions, then catalytic/ATP binding domains (which
137 phosphorylate a histidine on DHp). Response regulators include receiver domains (which receive the
138 phosphate from DHp) and effector domains. In some cases, the kinase and receiver reside on the same
139 molecule (hybrid histidine kinases), although two component systems are more common. Importantly, in
140 Tb927.9.3120 the regions corresponding to each domain are essentially complete and ordered as in hybrid
141 bacterial histidine kinases [23, 24] (see Fig. 2). This organization of a hybrid histidine kinase cassette
142 followed by a eukaryotic protein kinase domain is conserved in the Tb927.9.3120 orthologues in other
143 trypanosomatids, such as *T. cruzi* and *L. major*, and the bodonid *Bodo saltans* (data not shown). Together,
144 this provides intriguing evidence of a bacterial genetic incursion of a signaling cassette into a common
145 ancestor of bodonids and trypanosomatids. Accordingly, we propose to name this gene dual ancestor
146 kinase (*DAK*).

147 **Expression.** We examined the expression of these PKs using our previous genome-wide ribosome
148 profiling data from pleiomorphic slender form BF (isolated from mice) and cultured PF [25]. Ribosome
149 profiling provides a direct measure of protein production. In Fig. 3, the dark blue and red bars show the
150 abundance of ribosome-associated mRNA footprints of BF and PF respectively. For comparison, the
151 mRNA abundances are also shown (light blue and pink bars). Several of the PKs show higher protein
152 production in slender BF than in PF, with MEKK1 showing 3-fold more expression in slender BF and
153 eIF2Ka having 2-fold more. However, the most dramatic difference was for RDK1 with 7-fold more
154 mRNA and 40-fold more protein production in slender BF than in PF. Conversely, Tb927.9.3120 had
155 about twice as much protein production in PF than slender BF, although the mRNA levels are very
156 similar between stages. Most of the PKs were close to the median level of protein production for all non-
157 pseudogenes (224 reads per kb in BF and 202 in PF). However, three PKs showed lower protein
158 production, being in the lowest quartile of all PKs. LDK protein production was low in both stages; FHK
159 protein production was low in BF and very low in PF; and Tb927.9.12400 protein production was almost
160 absent in BF and very low in PF.

161 **Subcellular localization.** Previous work localized *T. brucei* LDK to the lipid droplet membrane [10] and
162 eIF2K2 to the flagellar pocket [11] (and its *T. cruzi* orthologue to endosomes [13]). Additionally, the
163 protein encoded by Tb927.10.1910 was localized to the cytoplasm and endocytic organelles in PF in the
164 TrypTag project [26]. We determined the localization of C-terminally tagged versions of the remaining
165 transmembrane PKs in single marker strain BF. A western blot (Fig. S2) shows the migration of the
166 tagged proteins in SDS gels, which corresponded reasonably well to the predicted sizes given in Table S1.
167 In the absence of antibodies specific to individual PKs, it is not possible to predict whether the expression
168 levels of the tagged protein are comparable to the endogenous levels. However, the very low levels of
169 FHK and Tb927.9.12400 revealed by ribosome profiling compared to their ready detection by western
170 blot (Fig. 3) suggest that the tagged versions of those PKs may be over-expressed.

171 <u>Many tagged TMD PKs localize to the ER.</u> As summarized in Table 1 and shown in Fig. 4, five of the
172 tagged PKs with predicted TMDs colocalized with the ER marker BiP. None of these PKs is classified as
173 related to the mammalian ER kinase PEK [7]. Staining of the tagged proteins is evident around the body
174 of the cell but does not extend along the flagellum after it passes the anterior end of the cell body. As with
175 BiP, some perinuclear staining is also seen; in most cases this is fainter than the peripheral staining.
176 RDK1 was previously shown to be associated with membranes and localized to the periphery of the
177 parasite [9]; our colocalization studies indicate that this peripheral localization is the ER. While it is clear
178 that these PKs enter the secretory system, the ER may not be their final destination, which could be
179 masked by potential over-expression.

180 MEKK1 is an integral membrane protein of the flagellum and flagellar pocket with kinase activity.
181 Immunofluorescence analysis showed that MEKK1-V5 is present along the flagellum, where it aligns
182 with PIFTC3, a component of the flagellar protein transport system [27] and is clearly distinct from the
183 flagellar K+ channel that also extends along the flagellum [28]. We also observed staining adjacent to the
184 kinetoplast, which was distinct from, but adjacent to, the depot of PIFTC3. When two kinetoplasts were
185 seen, two puncta of both PIFTC3 and MEKK1 were visible. Immunoelectron microscopy was performed
186 using PF expressing MEKK1 C-terminally tagged with HA epitopes. As shown in Fig. 6, gold particle
187 staining was present at the flagellar pocket (A, B) but not at the kinetoplast (C). In a dividing cell, both
188 flagellar pockets were stained. MEKK1-HA was also seen along the flagellum (Fig 6E). The MEKK1-HA
189 at the flagellar pocket may represent molecules in transit to the flagellum or a final destination, as is seen
190 for PIFTC3 [27] and (Figure 5).

191 To assess membrane association, we conducted cell extraction and fractionation of PF expressing
192 MEKK1-HA. The full-length protein migrated anomalously, somewhat faster than the 220 kDa marker
193 (the tagged protein is predicted to be 167 kDa). Membrane proteins are known to exhibit anomalous
194 migration on SDS-PAGE gels, migrating either slower or faster than predicted, with apparent molecular
195 masses averaging 80-113% of the predicted value [29]. The ~95 kDa V5-tagged fragment can be
196 disregarded since it is not seen in cells lysed directly in SDS sample buffer, and therefore represents a
197 degradation fragment. As shown in the immunoblot in Fig. 7, upon treatment of PF with digitonin to
198 release the cytosol, the intact kinase remained in the pellet fraction (P1). Subsequent treatment of the
199 digitonin pellet with sodium carbonate, pH 11, showed MEKK-V5 in the pellet (P2), demonstrating that it
200 is an integral membrane protein. Marker proteins PGKB (cytosolic), PGKA (glycosomal which shows
201 partial membrane association) [30] and vacuolar pyrophosphatase, TcVSP) (integral vacuolar membrane)
202 [31] verified the fractionation procedure.

203 To test for catalytic activity, anti-V5 immunoprecipitates from PF expressing MEKK1-V5, as well as
204 from the untransfected parental 29.13 line, were incubated with the exogenous substrate myelin basic
205 protein (MBP) in the presence of γ^{32}P-ATP. The proteins were then separated by SDS-PAGE and
206 analyzed by phosphorimaging (Fig. 7B, top) and western blot (Fig. 7B, bottom). MBP was
207 phosphorylated in the sample containing MEKK1-V5, but not the untransfected control, thereby
208 demonstrating that MEKK1 can phosphorylate an exogenous substrate.

209 FHK is an integral membrane protein of the flagellar pocket with kinase activity. Like MEKK1, FHK-V5
210 demonstrated staining near the kinetoplast, close to PIFTC3 upon immunofluorescence analysis of BF
211 (Fig. 8A). However, staining did not extend along the flagellum and little co-localization with BiP was
212 observed (Fig. 8B). Live PF expressing MEKK1-HA were incubated with biotinylated tomato lectin at 4°

213 C and then fixed for anti-HA staining (Fig. 8C). The low temperature allows lectin binding to the flagellar
214 pocket without internalization into the parasite. The HA staining was adjacent to and possibly overlapping
215 the tomato lectin signal. Fig. 8D depicts a PF parasite stained for DNA and FHK. Individual deconvolved
216 planes showed FHK between the nucleus and kinetoplast in what appears to be a basket-like structure.
217 Immunoelectron microscopy of PF demonstrated that the protein was localized to the flagellar pocket but
218 not to the flagellum or kinetoplast (Fig. 9A, enlarged in 9a), and occasionally staining is seen more
219 prominently on one side of the flagellar pocket (Fig. 9B, enlarged in 9b). Sometimes staining was
220 observed on vesicles close to the flagellar pocket, but only sporadically outside the region of the pocket
221 (Fig. 9 C, D).

222 PF expressing FHK-HA were fractionated as described above for MEKK1. Full-length FHK-HA was in
223 the digitonin pellet, and the carbonate-insoluble fraction, indicating it is an integral membrane protein
224 (Fig. 10A). As with MEKK1, the smaller degradation fragment can be disregarded since it was absent
225 from cells lysed in SDS sample buffer. To test for catalytic activity, immunoprecipitates from PF
226 expressing FHK-HA, as well as the untransfected, parental single marker line, were assayed as described
227 for MEKK1. As shown by phosphorimaging (Fig. 10B, top) and western blot (Fig. 10B, bottom), MBP
228 was phosphorylated in the sample containing FHK-HA, but not the untransfected control, providing
229 evidence of FHK catalytic activity.

230 **Discussion**

231 **A plethora of transmembrane domains**

232 In contrast to metazoan kinomes, which have large numbers of TMD PKs, protozoan kinomes vary
233 widely in their representation of TMD PKs. At one extreme, the *Giardia lamblia* genome encodes only
234 two predicted transmembrane PKs (two other PKs have predicted TMDs unlikely to be authentic since
235 they punctuate the catalytic domain). At the other extreme is *Entamoeba histolytica* with more than 80
236 predicted TMD PKs, most of which are related at the sequence level and some of which are likely non-
237 catalytic [32]. Like *E. histolytica, Plasmodium falciparum* has evolved a unique set of PKs, the FIKK
238 kinases, that comprise the majority of the parasite's 17 PKs with predicted TMDs. The FIKK kinases bear
239 the signature sequence for export out of the parasite [33], and at least some of them are important in
240 remodeling the host erythrocyte [34, 35]. Like *P. falciparum,* trypanosomatids fall between extremes of
241 *G. lamblia* and *E. histolytica*, with a paucity of PKs that bear TMDs compared to metazoans. These
242 trypanosomatid PKs are classified firmly with serine/threonine kinases as opposed to tyrosine kinases
243 characteristic of transmembrane PKs of animals [7]. Just as interesting, most of these trypanosomatid PKs
244 are predicted to have multiple membrane spanning domains, a feature that is extremely rare in eukaryotes.

245 To our knowledge, a single ePK domain protein in eukaryotes has been biochemically demonstrated to
246 have more than one TMD, lemur tail kinase 2 [36], but other members of that family of PKs are also
247 predicted to have two TMDs [37]. Interestingly, in perusing the *E. histolytica* genome database, we noted
248 a few PKs with two likely TMDs. Another interesting observation is that many bacterial histidine kinases
249 with several TMDs have been identified in genome-wide bioinformatic analyses [38]. These include the
250 5-TMD bearing *Staphylococcus aureus* LytS histidine kinase which acts as a sensor of membrane
251 potential [39]. Another example is *Bacillus subtilis* DesK, in which TMDs are involved in signaling
252 temperature-induced changes in membrane fluidity [40]. Thus, TMDs can modulate kinase activity in
253 response to environmental changes even when no extracellular ligand binding domains are present. It will
254 be interesting to determine if any of the TMDS in the *T. brucei* PKs examined here have such effects.

255 **Flagellar and flagellar pocket localization and function**

256 The localization of MEKK1 and FHK to the flagellum and flagellar pocket respectively raises the
257 question of what biochemical processes they may regulate. Initiation of stumpy development appears to
258 be triggered by the uptake of oligopeptides by the transporter GPR89 [41]. MEKK1 acts early in the
259 developmental pathway, which involves multiple additional kinases [8]. How the oligopeptide signal
260 intersects with MEKK1 is not clear given that GPR89 is distributed across the plasma membrane and is
261 not specifically localized to, or perhaps not present at all, at the flagellar membrane. However, other
262 molecules that may be involved in development are also localized to the flagella, such as adenylate
263 cyclases and phosphodiesterases that are present on the flagellum, as well as a calcium channel [42].

264 In trypanosomatids, the flagellar pocket is the site of the essential processes of exocytosis and
265 endocytosis. Therefore, the localization of FHK to the flagellar pocket could suggest a function in these
266 processes. RNAi data suggests that FHK is dispensable in BF [9, 43] (also corroborated by our
267 preliminary data), so it is unlikely that it functions as a global regulator of such essential processes.
268 Instead, its function may be focused on specific conditions (e.g., stress response) or certain pathways
269 within the broader categories of exocytosis, endocytosis and recycling of membrane molecules. Because
270 only the flagellar pocket is free of the densely packed, GPI-anchored variant surface protein coat which
271 covers the surface of the parasite and bears many distinct proteins, FHK could also be positioned at the
272 flagellar pocket to sense interaction with transmembrane proteins or even to biophysical changes in this
273 distinct membrane domain, such as those sensed by LytS and DesK.

274 **Signaling domains of likely bacterial origin**

275 There are numerous genes in trypanosomatids, especially those encoding metabolic enzymes, which are
276 more closely related at the amino acid sequence level to bacterial than to eukaryotic homologues,

277 providing evidence of lateral gene transfer. Our HHpred analysis showed that two *T. brucei* PKs have
278 regions predicted at >95% probability to fold similarly to bacterial signaling modules. FHK has a region
279 resembling ligand-sensing domains found on chemotaxis proteins and certain histidine kinases, but not on
280 eukaryotic proteins. DAK has cassette bearing four regions common to hybrid histidine kinases: a sensor,
281 a dimerization/phosphoacceptor, a catalytic domain and a receiver domain. These modular structures are
282 conserved in genomes across trypanosomatids and in the bodonid *Bodo saltans*, ruling out an artifactual
283 explanation and arguing for a functional and possibly regulatory role. While this combination of domains
284 is unusual, Uniprot searches do identify predicted proteins that possess both an ePK domain and a
285 histidine kinase cassette. Most of these predicted proteins are bacterial, but some are found in eukaryotes
286 (predominantly fungi). Those in eukaryotes almost exclusively have hybrid type histidine kinase domains
287 (i.e, with a receiver domain on the same molecule) as is seen on DAK. Few (if any) of these histidine-ePK
288 kinases have been explored functionally to understand how the domains interact and influence the
289 signaling properties of the protein. DAK's potential for histidine kinase activity that phosphorylates the
290 DHp region appears low since the conserved histidine is mutated. However, the aspartic acid in the
291 receiver domain that accepts the phosphate is still present. Clearly additional work will need to be done to
292 understand the roles of the two ancestral kinase regions on the kinase activity and ultimately function of
293 DAK [25].

294 **Materials and Methods**

295 **Parasites.** The work described uses PF 29-13 and single marker BF lines, which are derivatives of the *T.*
296 *brucei* 427 strain [44]. Both lines express T7 RNA polymerase and the tetracycline (Tet) repressor,
297 allowing for Tet-regulated expression of transfected genes. PF were grown in SDM-79 (JRH Biosciences)
298 supplemented with 15% fetal calf serum containing 15 μg/ml G418 and 50 μg/ml hygromycin to maintain
299 the T7 RNA polymerase and Tet repressor genes. BF were grown in HMI-9 with 2.5 μg/ml G418.
300 Plasmids were transfected into PF as described [44] and transfectants were selected with 1 μg/ml
301 puromycin. BF were transfected as described [45] and modified by [46]. BF transfectants were selected
302 with either 5 μg/ml hygromycin or blastocidin S depending on the plasmid vector.

303 **Plasmids and Cloning.** For expression of V5-tagged proteins in BF, we generated the plasmid pT7-3V5-
304 Hyg by replacing the GFP and lacZ stuffer region of pT7-GFP (kindly supplied by David Horn) [47] with
305 the multicloning site and 3V5 epitopes derived from pLEW79-3V5-Pac [10]. Expression was driven by a
306 tetracycline (Tet) regulated T7 promoter and the 3' UTR was derived from aldolase. For expression of
307 HA-tagged proteins in PF, either pLEW79-3V5-PAC or plasmid pLEW100v5-3HA-BSD were utilized.
308 The latter was created by replacing the luciferase gene in pLEW100v5-BSD (kindly supplied by George

309 Cross) with the multicloning sites derived from pLEW79-3V5-PAC and three HA epitope tags.
310 Expression was driven by a tetracycline (Tet) regulated PARP promoter and the 3' UTR was derived from
311 aldolase. The coding sequences for the PKs were amplified and PCR products were digested with the
312 restriction enzymes noted in the primer and ligated into appropriately digested vectors. The expression
313 construct for Tb927.9.3120 also included the endogenous splice acceptor. All primers are described in
314 Table S2.

315 **Western blots.** Cell lysates were generated, and proteins resolved by SDS-PAGE and transferred to
316 nitrocellulose as described [48]. V5-tagged proteins were detected with mouse monoclonal anti-V5
317 antibody (ThermoFisher) at 0.3 μg/ml. HA-tagged proteins were detected with mouse (Covance) or rat
318 (Roche) monoclonal anti-V5 antibodies at 1 μg/ml or 12.5 ng/ml respectively. Bound antibodies were
319 revealed with IRDye 800CW dye-conjugated goat anti-mouse Ig (Li-COR) at 25 ng/ml and data was
320 visualized on a Li-COR Odyssey.

321 **Immunofluorescence analysis**. IFAs were performed as previously described [48]. In brief, BF parasites
322 were prefixed in 4% paraformaldehyde for 5 min on ice prior to placing on poly-L-lysine coverslips. The
323 V5 epitope tag was detected by using mouse monoclonal anti-V5 antibody (Invitrogen) at 1 ug/ml,
324 followed by goat anti-mouse IgG conjugated with fluorescein isothiocyanate (FITC) (Southern
325 Biotechnology). Additional antibodies used for colocalization included antibodies directed against BiP
326 [49] (kindly supplied by Jay Bangs), used at 1:400; PIFTC3 [27] (kindly supplied by Elisabetta Ullu),
327 used at 1:1000; TcCat [28] (kindly supplied by Roberto DeCampo), used at 1:250; YL1/2 (Gene-Tex),
328 used at 1 μg/ml. To visualize the flagellar pocket, pre-cooled cells were incubated at 4°C with
329 biotinylated tomato lectin (Vector Laboratories) at 2 μg/ml. After fixation, tomato lectin was visualized
330 with 2 μg/ml streptavidin conjugated to either Texas Red or Alexa Fluor 488 (ThermoFisher). Dye-
331 conjugated secondary antibodies (Southern Biotechnology) were used at 2 μg/ml. Images were scaled to
332 span the graph of signal intensity of the image field.

333 **Immunoelectron microscopy.** Preparations of parasites were fixed in 4% paraformaldehyde (Electron
334 Microscopy Sciences, PA) in 0.25 M HEPES (pH 7.4) for 1 h at room temperature, then in 8%
335 paraformaldehyde in the same buffer overnight at 4oC. They were infiltrated, frozen and sectioned as
336 previously described [50]. The sections were immunolabeled with rat anti-HA antibodies (1:50 in
337 PBS/1% fish skin gelatin), then with anti-mouse IgG antibodies, followed directly by 10 nm protein A-
338 gold particles (Department of Cell Biology, Medical School, Utrecht University, the Netherlands) before
339 examination with a Philips CM120 Electron Microscope (Eindhoven, the Netherlands) under 80 kV.

340 **Cell fractionation and Kinase assays.** PF expressing HA-tagged proteins washed in PBS containing 10
341 mM glucose. They were permeabilized with digitonin and the organellar pellet was extracted with sodium
342 carbonate as described [51] except that Complete Protease tablets (Roche) were included for both
343 digitonin permeabilization and carbonate extraction, to prevent protein degradation.

344 Cell lysates from PF cells expressing either V5-tagged MEKK1 or HA-tagged FHK along with the
345 untransfected parental line 29.13 were prepared as described [52]. Epitope tagged proteins were
346 immunoprecipitated from cell lysate prepared from 10^8 cells. Kinase assays were done as described [53]
347 using ^{32}PγATP with myelin basic protein as an exogenous substrate. Reactions were resolved by SDS-
348 PAGE and transferred to nitrocellulose and labeled proteins detected by phosphorimaging. Blots were
349 subsequently probed with antibodies directed against either V5 or HA.

350 **Acknowledgements**: This work was supported in part by a grant 5R21AI101424 from the National
351 Institutes of Health and by Seattle Children's Research Institute.

352 **Author contributions**

353 Concept and experimental design were done by B.C.J and M.P. Experiments were performed by B.C.J,
354 P.V. and J.F except electron microscopy done by I.C. Manuscript was written by M.P. and B.C.J. All
355 authors have reviewed the manuscript.

356 **Conflicts of interest**

357 The authors declare no competing interest.

358

359
360

361 **References**
362

363 1. El-Sayed, N.M., et al., The genome sequence of *Trypanosoma cruzi*, etiologic agent of Chagas
364 disease. Science, 2005. **309**(5733): p. 409-415.
365 2. Alexandre, S., et al., Families of adenylate cyclase genes in *Trypanosoma brucei*. Mol. Biochem.
366 Parasitol, 1996. **77**(2): p. 173-182.
367 3. Norouzi, S., et al., Zinc transporters and insulin resistance: therapeutic implications for type 2
368 diabetes and metabolic disease. J. Biomed. Sci, 2017. **24**(1): p. 87.
369 4. Bon, N., et al., Phosphate (Pi)-regulated heterodimerization of the high-affinity sodium-
370 dependent Pi transporters PiT1/Slc20a1 and PiT2/Slc20a2 underlies extracellular Pi sensing
371 independently of Pi uptake. J. Biol Chem, 2017.
372 5. Henjakovic, M., et al., Human organic anion transporter 2 is distinct from organic anion
373 transporters 1 and 3 with respect to transport function. Am. J. Physiol. Renal Physiol, 2015.
374 **309**(10): p. F843-F851.
375 6. Dean, S., et al., A surface transporter family conveys the trypanosome differentiation signal.
376 Nature, 2009. **459**(7244): p. 213-7.
377 7. Parsons, M., et al., Comparative analysis of the kinomes of three pathogenic trypanosomatids:
378 *Leishmania major*, *Trypanosoma brucei* and *Trypanosoma cruzi*. BMC. Genomics, 2005. **6**: p.
379 127.
380 8. McDonald, L., et al., Non-linear hierarchy of the quorum sensing signalling pathway in
381 bloodstream form African trypanosomes. PLoS Pathog, 2018. **14**(6): p. e1007145.
382 9. Jones, N.G., et al., Regulators of *Trypanosoma brucei* cell cycle progression and differentiation
383 identified using a kinome-wide RNAi screen. PLoS Pathog, 2014. **10**(1): p. e1003886.
384 10. Flaspohler, J.A., et al., A novel protein kinase localized to lipid droplets is required for droplet
385 biogenesis in trypanosomes. Eukaryot. Cell, 2010. **9**(11): p. 1702-1710.
386 11. Moraes, M.C., et al., A novel membrane-bound eIF2 alpha kinase in the flagellar pocket of
387 *Trypanosoma brucei*. Eukaryot. Cell, 2007. **6**: p. 1979-1991.
388 12. Chow, C., et al., Promastigote to amastigote differentiation of *Leishmania* is markedly delayed in
389 the absence of PERK eIF2alpha kinase-dependent eIF2alpha phosphorylation. Cell Microbiol,
390 2011. **13**(7): p. 1059-77.
391 13. da Silva Augusto, L., et al., A membrane-bound eIF2 alpha kinase located in endosomes is
392 regulated by heme and controls differentiation and ROS levels in *Trypanosoma cruzi*. PLoS
393 Pathog, 2015. **11**(2): p. e1004618.
394 14. Alsford, S., et al., High-throughput decoding of antitrypanosomal drug efficacy and resistance.
395 Nature, 2012. **482**(7384): p. 232-6.
396 15. Shao, S. and R.S. Hegde, Membrane protein insertion at the endoplasmic reticulum. Annu Rev
397 Cell Dev Biol, 2011. **27**: p. 25-56.
398 16. Lee, H. and H. Kim, Membrane topology of transmembrane proteins: determinants and
399 experimental tools. Biochem Biophys Res Commun, 2014. **453**(2): p. 268-76.
400 17. Paindavoine, P., et al., A gene from the variant surface glycoprotein expression site encodes one
401 of several transmembrane adenylate cyclases located on the flagellum of *Trypanosoma brucei*.
402 Mol Cell Biol, 1992. **12**(3): p. 1218-25.
403 18. Mahajan, A., et al., Structure and function of the phosphothreonine-specific FHA domain. Sci
404 Signal, 2008. **1**(51): p. re12.
405 19. Zimmermann, L., et al., A Completely Reimplemented MPI Bioinformatics Toolkit with a New
406 HHpred Server at its Core. J Mol Biol, 2018. **430**(15): p. 2237-2243.
407 20. Corral-Lugo, A., et al., High-Affinity Chemotaxis to Histamine Mediated by the TlpQ
408 Chemoreceptor of the Human Pathogen *Pseudomonas aeruginosa*. mBio, 2018. **9**(6).
409 21. Zhang, Z. and W.A. Hendrickson, Structural characterization of the predominant family of
410 histidine kinase sensor domains. J Mol Biol, 2010. **400**(3): p. 335-53.

411 22. Jackson, A.P., et al., Kinetoplastid Phylogenomics Reveals the Evolutionary Innovations
412 Associated with the Origins of Parasitism. Curr Biol, 2016. **26**(2): p. 161-172.
413 23. Wang, C., et al., Mechanistic insights revealed by the crystal structure of a histidine kinase with
414 signal transducer and sensor domains. PLoS Biol, 2013. **11**(2): p. e1001493.
415 24. Dubey, B.N., et al., Hybrid histidine kinase activation by cyclic di-GMP-mediated domain
416 liberation. Proc Natl Acad Sci U S A, 2020. **117**(2): p. 1000-1008.
417 25. Jensen, B.C., et al., Extensive stage-regulation of translation revealed by ribosome profiling of
418 *Trypanosoma brucei*. BMC Genomics, 2014. **15**(1): p. 911.
419 26. Dean, S., J.D. Sunter, and R.J. Wheeler, TrypTag.org: A Trypanosome Genome-wide Protein
420 Localisation Resource. Trends Parasitol, 2017. **33**(2): p. 80-82.
421 27. Franklin, J.B. and E. Ullu, Biochemical analysis of PIFTC3, the *Trypanosoma brucei* orthologue
422 of nematode DYF-13, reveals interactions with established and putative intraflagellar transport
423 components. Mol. Microbiol, 2010. **78**(1): p. 173-186.
424 28. Jimenez, V. and R. Docampo, Molecular and electrophysiological characterization of a novel
425 cation channel of *Trypanosoma cruzi*. PLoS Pathog, 2012. **8**(6): p. e1002750.
426 29. Rath, A. and C.M. Deber, Correction factors for membrane protein molecular weight readouts on
427 sodium dodecyl sulfate-polyacrylamide gel electrophoresis. Anal Biochem, 2013. **434**(1): p. 67-
428 72.
429 30. Parker, H.L., et al., Three genes and two isozymes: Gene conversion and the
430 compartmentalization and expression of the phosphoglycerate kinases of *Trypanosoma*
431 (*Nannomonas*) *congolense*. Mol. Biochem. Parasitol, 1995. **69**: p. 269-279.
432 31. Galizzi, M., et al., Evidence for the role of vacuolar soluble pyrophosphatase and inorganic
433 polyphosphate in *Trypanosoma cruzi* persistence. Mol Microbiol, 2013. **90**(4): p. 699-715.
434 32. Beck, D.L., et al., Identification and gene expression analysis of a large family of transmembrane
435 kinases related to the Gal/GalNAc lectin in *Entamoeba histolytica*. Eukaryot Cell, 2005. **4**(4): p.
436 722-32.
437 33. Schneider, A.G. and O. Mercereau-Puijalon, A new Apicomplexa-specific protein kinase family:
438 multiple members in *Plasmodium falciparum*, all with an export signature. BMC Genomics,
439 2005. **6**(1): p. 30.
440 34. Davies, H., et al., An exported kinase family mediates species-specific erythrocyte remodelling
441 and virulence in human malaria. Nat Microbiol, 2020. **5**(6): p. 848-863.
442 35. Nunes, M.C., et al., *Plasmodium falciparum* FIKK kinase members target distinct components of
443 the erythrocyte membrane. PLoS One, 2010. **5**(7): p. e11747.
444 36. Nixon, A., et al., Determination of the membrane topology of lemur tyrosine kinase 2 (LMTK2)
445 by fluorescence protease protection. Am J Physiol Cell Physiol, 2013. **304**(2): p. C164-9.
446 37. Hisanaga, S.I., et al., LMTK1, a Novel Modulator of Endosomal Trafficking in Neurons. Front
447 Mol Neurosci, 2020. **13**: p. 112.
448 38. Anantharaman, V. and L. Aravind, Application of comparative genomics in the identification and
449 analysis of novel families of membrane-associated receptors in bacteria. BMC Genomics, 2003.
450 **4**(1): p. 34.
451 39. Patel, K. and D. Golemi-Kotra, Signaling mechanism by the *Staphylococcus aureus* two-
452 component system LytSR: role of acetyl phosphate in bypassing the cell membrane electrical
453 potential sensor LytS. F1000Res, 2015. **4**: p. 79.
454 40. Fernandez, P., et al., Transmembrane Prolines Mediate Signal Sensing and Decoding in *Bacillus*
455 *subtilis* DesK Histidine Kinase. mBio, 2019. **10**(6).
456 41. Rojas, F., et al., Oligopeptide Signaling through TbGPR89 Drives Trypanosome Quorum
457 Sensing. Cell, 2019. **176**(1-2): p. 306-317 e16.
458 42. Kelly, F.D., P.A. Yates, and S.M. Landfear, Nutrient sensing in *Leishmania*: Flagellum and
459 cytosol. Mol Microbiol, 2020.
460 43. Fernandez-Cortes, F., et al., RNAi screening identifies *Trypanosoma brucei* stress response
461 protein kinases required for survival in the mouse. Sci Rep, 2017. **7**(1): p. 6156.

462 44. Wirtz, E., et al., A tightly regulated inducible expression system for conditional gene knock-outs
463 and dominant-negative genetics in *Trypanosoma brucei*. Mol Biochem Parasitol, 1999. **99**(1): p.
464 89-101.
465 45. Carruthers, V.B. and G.A.M. Cross, High-efficiency clonal growth of bloodstream- and insect-
466 form *Trypanosoma brucei* on agarose plates. Proc. Natl. Acad. Sci. USA, 1992. **89**: p. 8818-8821.
467 46. Schnaufer, A., et al., An RNA ligase essential for RNA editing and survival of the bloodstream
468 form of *Trypanosoma brucei*. Science, 2001. **291**(5511): p. 2159-2162.
469 47. Alsford, S., et al., Tagging a *T. brucei* RRNA locus improves stable transfection efficiency and
470 circumvents inducible expression position effects. Mol Biochem Parasitol, 2005.
471 48. Jensen, B.C., et al., The NOG1 GTP-binding protein is required for biogenesis of the 60S
472 ribosomal subunit. J Biol Chem, 2003. **278**: p. 32204-32211.
473 49. Bangs, J.D., et al., Molecular cloning and cellular localization of a BiP homologue in
474 *Trypanosoma brucei*. Divergent ER retention signals in a lower eukaryote. J. Cell Sci, 1993. **105**:
475 p. 1101-1113.
476 50. Folsch, H., et al., Distribution and function of AP-1 clathrin adaptor complexes in polarized
477 epithelial cells. J Cell Biol, 2001. **152**(3): p. 595-606.
478 51. Saveria, T., et al., Conservation of PEX19-binding motifs required for protein targeting to
479 mammalian peroxisomal and trypanosome glycosomal membranes. Eukaryot Cell, 2007. **6**(8): p.
480 1439-1449.
481 52. Das, A., et al., Distinct domains of a nucleolar protein mediate protein kinase binding, interaction
482 with nucleic acids and nucleolar localization. Journal of Cell Science, 1998. **111 (Pt 17)**: p.
483 2615-2623.
484 53. Park, J.H., et al., Molecular cloning of *Trypanosoma brucei* CK2 catalytic subunits: the alpha
485 isoform is nucleolar and phosphorylates the nucleolar protein Nopp44/46. Molecular and
486 Biochemical Parasitology, 2002. **119**(1): p. 97-106.

487

488 **Table 1 Summary of localization studies**

GeneID/name	**TrypTag** PF[a], endogenous	**other studies**	**This study** BF, ectopic, C-terminal tag
Tb927.2.2720 MEKK1	N -faint[b], cytoplasm and flagellum; C - faint, cytoplasmic, reticular		Flagellum, flagellar pocket; similar in PF
Tb927.3.5650	nd		ER
Tb927.4.2500 eIF2K2	N - very faint, cytoplasmic puncta; C - nd	Flagellar pocket and endosomes [11]	nd
Tb927.5.3150	N- nd; C – reticulated with occasional bright puncta		ER
Tb927.7.5220 FHK	nd		At or near flagellar pocket, similar in PF
Tb927.9.3120	nd		ER
Tb927.9.12400	nd		ER
Tb927.10.1910	N - faint, endocytic and cytoplasm; C -ND		nd

Tb927.11.8940 LDK	nd	Lipid droplets [10]	nd
Tb927.11.14070 RDK1	nd	Periphery [9]	ER

[a] TrypTag: in situ tags the test protein with neon-green at the N- or C-terminus of the protein for expression in PF [26].
[b]Faint, 10-20th percentile of all lines expressing tagged proteins; very faint, <10th percentile. Note that these are all fainter than the parental line, but in cases where proteins are localized to specific organelles, localization can often be visualized.

Figure Legends

Figure 1. Schematics of *T. brucei* protein kinases predicted to bear transmembrane domains. TMDs predicted by both TMHMM and CCTOP are marked with red bars (one predicted by TMHMM only is marked with a red X); additional TMDs predicted by CCTOP are marked by red arrowheads. Predicted signal sequences are indicated by a red asterisk. Light blue regions are ePK Pfam domains. Yellow bars depict other domains: PAS motif (P), forkhead associated domain (F), nucleotide cyclase-like domain (NTC), Kelch propeller blade (K). Light green bars demarcate regions with predicted structural similarity to known structures revealed by HHpred. Bacterial DHp, catalytic, and receiver domains characteristic of histidine kinases (D-C-R) in Tb927.9.3120, as well as bacterial sensor/receptor domains (S/R) and adenylyl/guanylyl cyclases (AGC) in RDK1, exhibited probabilities >95% (see Figs. 2 and S2 for details). The PAS-like domain in FHK was detected with >90% probability. Length of the predicted protein in amino acids is indicated.

Fig. 2. HHpred analysis of Tb927.9.3120 shows evidence of ancient domains. The PK domain (aa 737-980) is not shown. Red ovals – transmembrane domains predicted by TMHMM and CCTOP. Each bar below the gene model represents the top hits by HHpred. The color of the arrows mark descriptions matching the hits. The description includes the PDB number and chain designation (Hit), a description of the PDB entry including related PDB entries (Name), the probability of the hit based on the Hidden Markov Model (Probability), the probability of the match in an unrelated database (E-value), score for the secondary structure prediction (SS), number of amino acids aligned (Col), and the total length of the target in PDB (Target Length). The documentation for HHpred considers “Probability" the most important criterion with our hits meeting at least one of the twomost stringent criteria: having a score >95% or having a score >50% and making reasonable biological sense [19].

517 **Fig. 3. Protein production and mRNA levels of TMD PKs.** Protein production was measured by
518 ribosome profiling and mRNA levels were measured in the same biological samples (three replicates
519 each). Data is shown as reads per kb and is derived from [25].

520 **Figure 4. Localization of V5-tagged predicted membrane kinases to the ER in bloodstream form *T.***
521 ***brucei*.** BF were fixed and stained with primary antibodies. Bound antibodies were revealed with
522 secondary fluorochrome-coupled antibodies. Green, V5-tagged proteins, Red, anti-BiP, Blue, DAPI;
523 Merge, all three colors. Each series shows a single deconvolved plane, except the DIC image, which is a
524 projection. All images are shown at the same magnification. Bar, 5 μm.

525 **Figure 5. Immunofluorescence localization of MEKK1-V5 (Tb927.2.2720) in *T. brucei* bloodstream**
526 **forms.** Top, co-staining with tomato lectin (TL, green) at 4°, which marks the flagellar pocket. Note that
527 punctate staining continues to the end of the flagellum. Middle, co-staining with antibody *to T. brucei*
528 PIFCT3 (red), a component of the flagellar transport system. Bottom, co-staining with antibody to a K+
529 channel protein of *T. cruzi* (left, red) and with monoclonal antibody YL2 (right, red) which detects basal
530 bodies. The latter shows a cell with two kinetoplasts and appears to be in early mitosis. Each series shows
531 a single deconvolved plane, except DIC images, which are projection. All images, except enlargements,
532 are shown at the same magnification (bar, 5 μm). Enlargements show detail near the kDNA. N, nucleus;
533 k, kDNA.

534 **Figure 6. Localization of MEKK1-HA to the flagellum and flagellar pocket by immunoelectron**
535 **microscopy.** PF expressing MEKK1 C-terminally tagged with HA epitopes were stained with anti-HA,
536 and staining revealed by protein-A gold 10 nm particles. **A)** The gold staining is on the flagellar pocket
537 (FP) membrane, flagellum (F), but absent from the mitochondrion (m). **B)** staining is observed at the base
538 of the flagellar pocket at the basal bodies (BB). **C)** no staining of the kinetoplast (k) is seen. **D)** in a
539 dividing cell, both flagellar pockets are stained. **E)** the external portion of the flagellum is also stained.
540 Bars, 100 nm.

541 **Figure 7. MEKK1 is an integral membrane protein which has protein kinase activity. A)** Cell
542 fractionation. PF cells expressing MEKK1-HA were fractionated by digitonin treatment followed by
543 carbonate extraction. After separation by SDS-PAGE and blotting, the blots were probed with mouse anti-
544 HA (green) and rabbit anti-phosphoglycerate kinase (red) which detects the 56 kDa glycosomal form
545 (PGKA) and the 47 kDa cytosolic isoform (PGKB). A parallel blot was also incubated with antibody to
546 the acidocalcisome membrane protein vacuolar phosphatase (VP). SDS, SDS lysate; T, total after
547 incubation with digitonin; S1, digitonin supernatant; P1, digitonin pellet; S2, carbonate supernatant; P2,
548 carbonate pellet. Lanes contain fractions from 3×10^6cells. **B)** Kinase activity. Immunoprecipitated

549 MEKK1 from PF was incubated with γ ^{32}P-ATP and the exogenous substrate myelin basic protein (MBP),
550 followed by SDS-PAGE and transfer to nitrocellulose. A control immunoprecipitation used the
551 untransfected parental line (29.13). Top: phosphorimaging demonstrates phosphorylation of MBP.
552 Bottom: the blot was probed with anti-V5 mAb demonstrating the pulldown of the tagged protein.

553 **Figure 8. Predominant localization of epitope-tagged FHK near the kinetoplast. A, B)** BF expressing
554 FHK-V5 and co-stained with DAPI, anti-V5 antibodies, and either anti-PIFTC3 (A) or anti-BiP (B).
555 Enlargement shows region around kDNA. The cell in (A) has duplicated both its nucleus (N) and kDNA
556 (k) and is undergoing cytokinesis as evidenced by the presence of two flagella (F). The cell in panel B has
557 an elongated, slightly V-shaped kinetoplast, indicating it is undergoing kinetoplast division and is in
558 nuclear S phase. Note that a point of FHK-staining occurs at either pole of the elongated kDNA. **C)** PF
559 expressing FHK-HA were incubated with biotinylated-tomato lectin (TL) at 4° and fixed prior to staining
560 with DAPI, avidin and anti-HA. Enlargement shows region around kDNA. **D)** Whole cell and enlarged
561 serial planes (numbered) of a DAPI-stained PF cell expressing FHK-HA. All images (except
562 enlargements) are at the same magnification. Bar = 5 μm.

563 **Fig. 9. Localization of FHK-HA to the flagellar pocket by immunoelectron microscopy**

564 Procyclic form parasites expressing FHK C-terminally tagged with HA epitopes were stained with anti-
565 HA revealed by protein-A gold 10 nm particles. **A)** The gold staining is on the flagellar pocket (FP)
566 membrane but absent from the flagellum (F) and mitochondrion (m). Enlargement of the marked region is
567 shown in panel a. **B)** Staining is predominantly at the flagellar pocket, and often one side shows more
568 abundant FHK. Enlargement of the marked region is shown in panel b. **C)** The staining is sometimes seen
569 on vesicles close to the FP. **D**) Occasional parasites showed staining outside the flagellar pocket. Bars,
570 100 nm.

571 **Figure 10. FHK is an integral membrane protein with protein kinase activity. A)** Cell fractionation
572 and immunoblotting were as described in Fig. 7. **B)** Kinase activity as described in Fig. 9. FHK-HA was
573 immunoprecipitated from PF and incubated with γ ^{32}P-ATP and MBP. A negative control
574 immunoprecipitation was performed using the untransfected parental line 29.13. Top: phosphorimaging
575 demonstrates phosphorylation of MBP. Bottom: the blot was probed with anti-HA mAb demonstrating
576 the pulldown of the tagged protein.

577

578 # List of supplementary information

579 **Supplementary tables**

580 Table S1. TriTryp orthologues - transmembrane domains, signal sequences, and additional
581 domains

582 Table S2. Primers

583 **Supplementary figures**

584 Fig. S1. RDK1 structural similarities identified by HHpred

585 Figure S2. Western blot showing expression of epitope-tagged PKs in *T. brucei* bloodstream
586 forms.

587

588

589

590

Figure 1

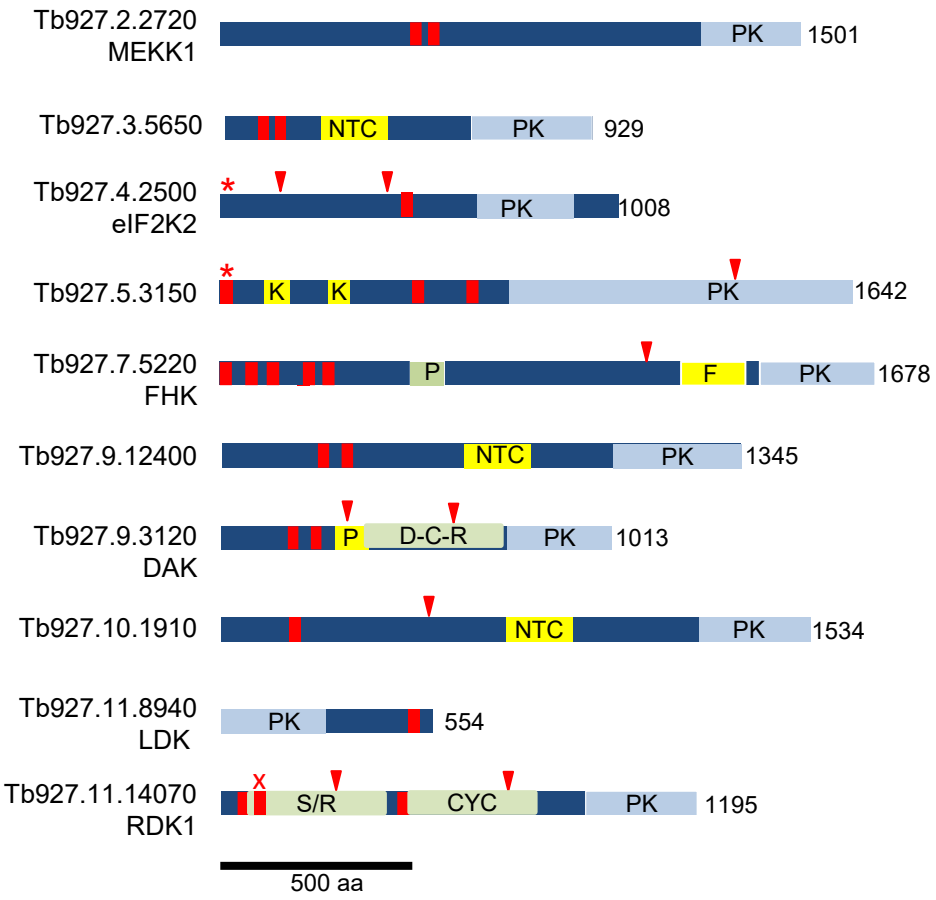

Figure 1. Schematics of *T. brucei* protein kinases predicted to bear transmembrane domains. TMDs predicted by both TMHMM and CCTOP are marked with red bars (one predicted by TMHMM only is marked with a red X); additional TMDs predicted by CCTOP are marked by red arrowheads. Predicted signal sequences are indicated by a red asterisk. Light blue regions are ePK Pfam domains. Yellow bars depict other domains: PAS motif (P), forkhead associated domain (F), nucleotide cyclase-like domain (NTC), Kelch propeller blade (K). Light green bars demarcate regions with predicted structural similarity to known structures revealed by HHpred. Bacterial DHp, catalytic, and receiver domains characteristic of histidine kinases (D-C-R) in Tb927.9.3120, as well as bacterial sensor/receptor domains (S/R) and adenylyl/guanylyl cyclases (AGC) in RDK1, exhibited probabilities >95% (see Figs. 2 and S2 for details). The PAS-like domain in FHK was detected with >90% probability. Length of the predicted protein in amino acids is indicated.

Figure 2

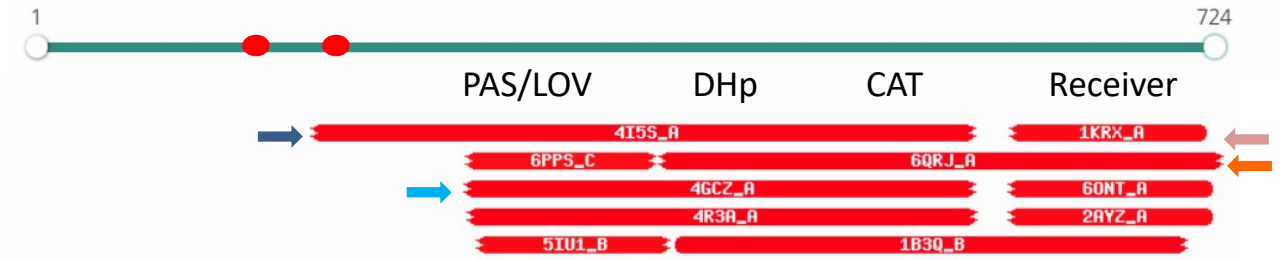

Nr	Hit	Name	Probability	E-value	SS	Cols	Target Length
1	4I5S_A	Putative histidine kinase CovS ; HISTIDINE KINASE, VICK, HAMP, PAS; 3.3A {Streptococcus mutans serotype c}; Related PDB entries: 4I5S_B	99.95	2.2e-26	25.8	372	450
2	6QRJ_A	Hybrid kinase; Cyclic di-GMP, second messenger, hybride; HET: ANP; 2.65A {Caulobacter vibrioides CB15}	99.94	1.5e-24	29.6	301	484
3	4GCZ_A	Blue-light photoreceptor, Sensor protein fixL; photoreceptor, signal transduction, two-component system; HET: MSE, SO4, ADP, FMN; 2.3A {Bacillus subtilis}; Related PDB entries: 4GCZ_B	99.89	8.6e-21	31.8	294	385
4	4R3A_A	Blue-light-activated histidine kinase 2 (E.C.2.7.13.3); light-activated, LOV domain, histidine kinase; HET: RBF, ANP; 2.92A {Erythrobacter litoralis HTCC2594}; Related PDB entries: 4R3A_B	99.88	2.8e-20	31.5	296	352
5	1B3Q_B	CHEMOTAXIS PROTEIN CHEA; HISTINE KINASE, SIGNAL TRANSDUCTION, CHEMOTAXIS; 2.6A {Thermotoga maritima} SCOP: d.122.1.3, a.30.2.1, b.40.7.1; Related PDB entries: 1B3Q_A 3JA6_C 3JA6_E	99.88	9.6e-22	19	281	379
42	1KRX_A	NITROGEN REGULATION PROTEIN NR(I); two component signal transduction, receiver; HET: BEF; NMR {Salmonella typhimurium} SCOP: c.23.1.1; Related PDB entries: 1DC7_A 1DC8_A 1J56_A 1KRW_A 2MSK_A 2MSL_A 1NTR_A	98.73	2.3e-7	13.2	114	124

Fig. 2. HHpred analysis of Tb927.9.3120 shows evidence of ancient domains. The PK domain (aa 737-980) is not shown. Red ovals – transmembrane domains predicted by TMHMM and CCTOP. Each bar below the gene model represents the top hits by HHpred. The color of the arrows mark descriptions matching the hits. The description includes the PDB number and chain designation (Hit), a description of the PDB entry including related PDB entries (Name), the probability of the hit based on the Hidden Markov Model (Probability), the probability of the match in an unrelated database (E-value), score for the secondary structure prediction (SS), number of amino acids aligned (Col), and the total length of the target in PDB (Target Length). The documentation for HHpred considers “Probability" the most important criterion with our hits meeting at least one of the twomost stringent criteria: having a score >95% or having a score >50% and making reasonable biological sense [19].

Figure 3

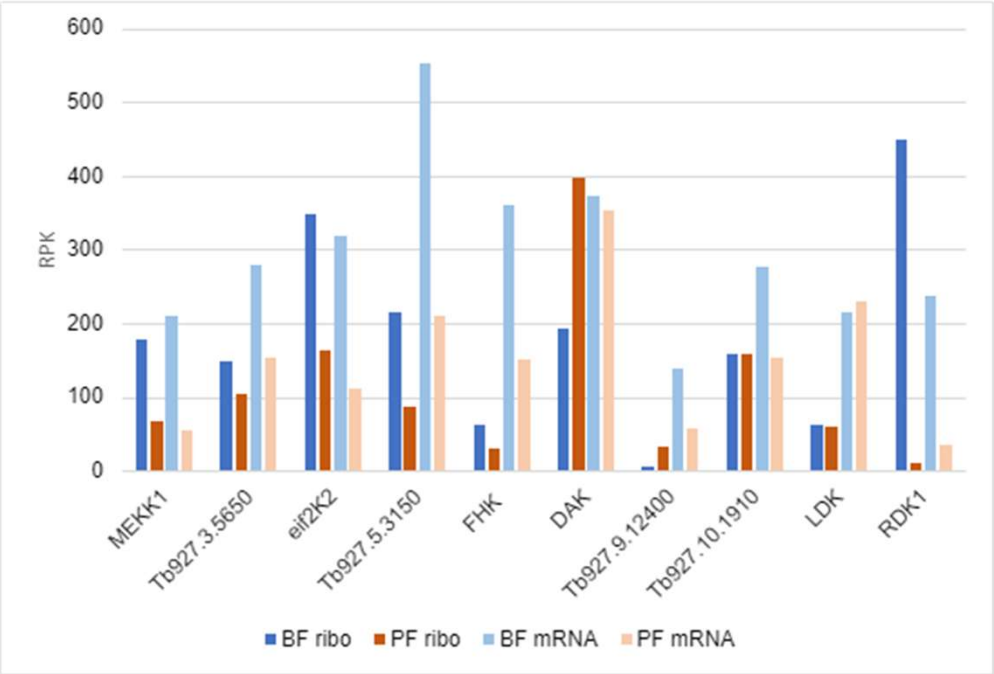

Fig. 3. Protein production and mRNA levels of TMD PKs. Protein production was measured by ribosome profiling and mRNA levels were measured in the same biological samples (three replicates each). Data is shown as reads per kb and is derived from [25].

Figure 4

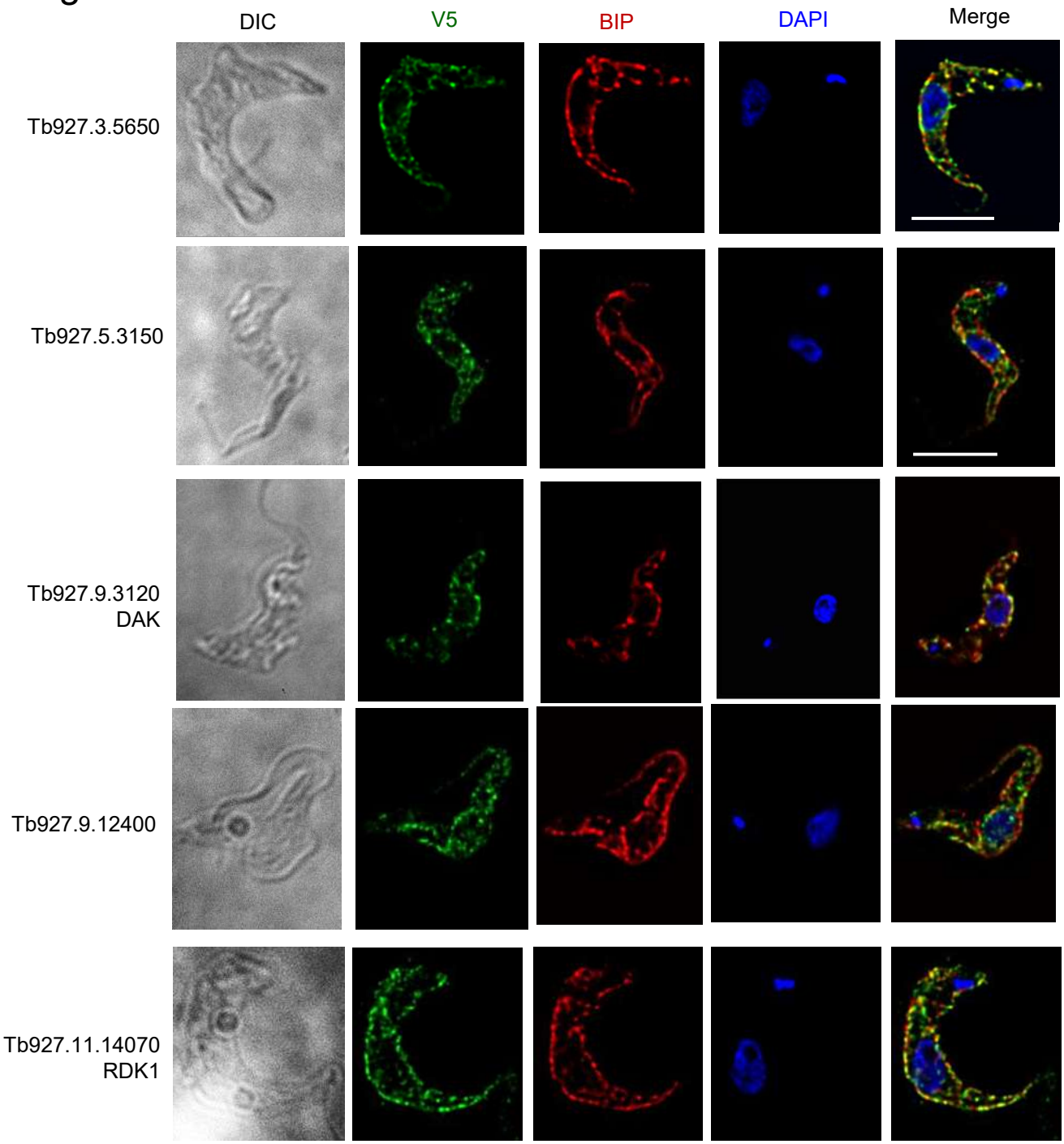

Figure 4. Localization of V5-tagged predicted membrane kinases to the ER in bloodstream form *T. brucei*. BF were fixed and stained with primary antibodies. Bound antibodies were revealed with secondary fluorochrome-coupled antibodies. Green, V5-tagged proteins, Red, anti-BiP, Blue, DAPI; Merge, all three colors. Each series shows a single deconvolved plane, except the DIC image, which is a projection. All images are shown at the same magnification. Bar, 5 µm.

Figure 5

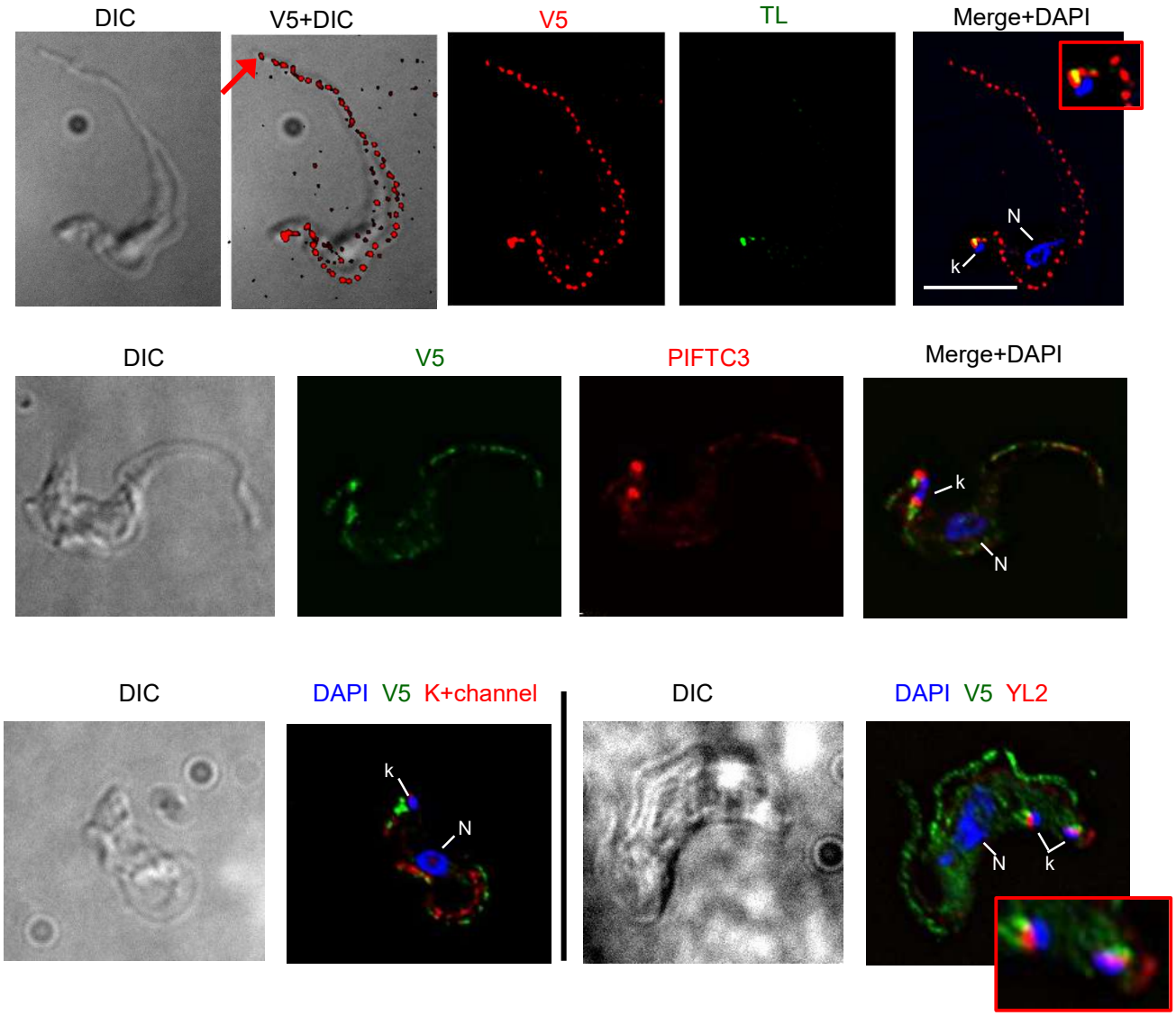

Figure 5. Immunofluorescence localization of MEKK1-V5 (Tb927.2.2720) in *T. brucei* bloodstream forms. Top, co-staining with tomato lectin (TL, green) at 4°, which marks the flagellar pocket. Note that punctate staining continues to the end of the flagellum. Middle, co-staining with antibody to T. brucei PIFCT3 (red), a component of the flagellar transport system. Bottom, co-staining with antibody to a K+ channel protein of T. cruzi (left, red) and with monoclonal antibody YL2 (right, red) which detects basal bodies. The latter shows a cell with two kinetoplasts and appears to be in early mitosis. Each series shows a single deconvolved plane, except DIC images, which are projection. All images, except enlargements, are shown at the same magnification (bar, 5 μm). Enlargements show detail near the kDNA. N, nucleus; k, kDNA.

Figure 6

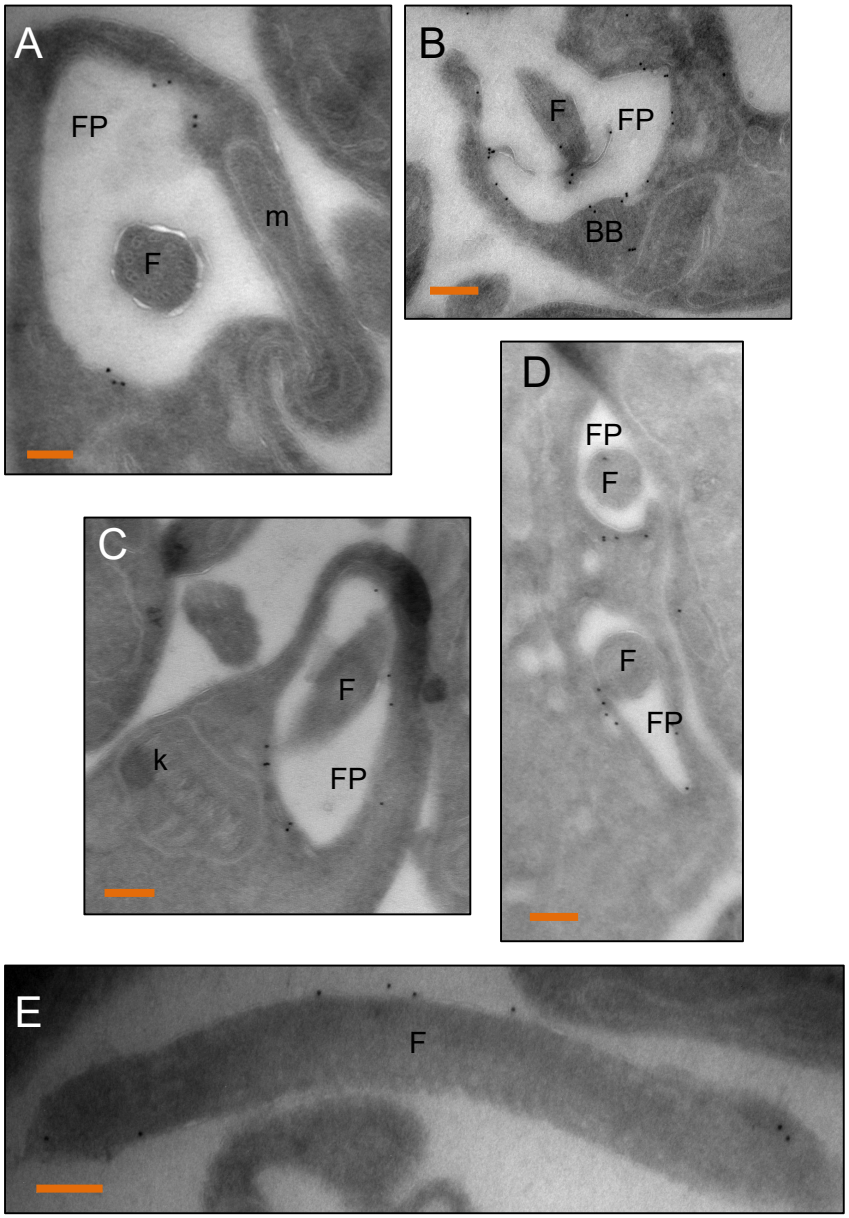

Figure 6. Localization of MEKK1-HA to the flagellum and flagellar pocket by immunoelectron microscopy. PF expressing MEKK1 C-terminally tagged with HA epitopes were stained with anti-HA, and staining revealed by protein-A gold 10 nm particles. A) The gold staining is on the flagellar pocket (FP) membrane, flagellum (F), but absent from the mitochondrion (m). B) staining is observed at the base of the flagellar pocket at the basal bodies (BB). C) no staining of the kinetoplast (k) is seen. D) in a dividing cell, both flagellar pockets are stained. E) the external portion of the flagellum is also stained. Bars, 100 nm.

Figure 7

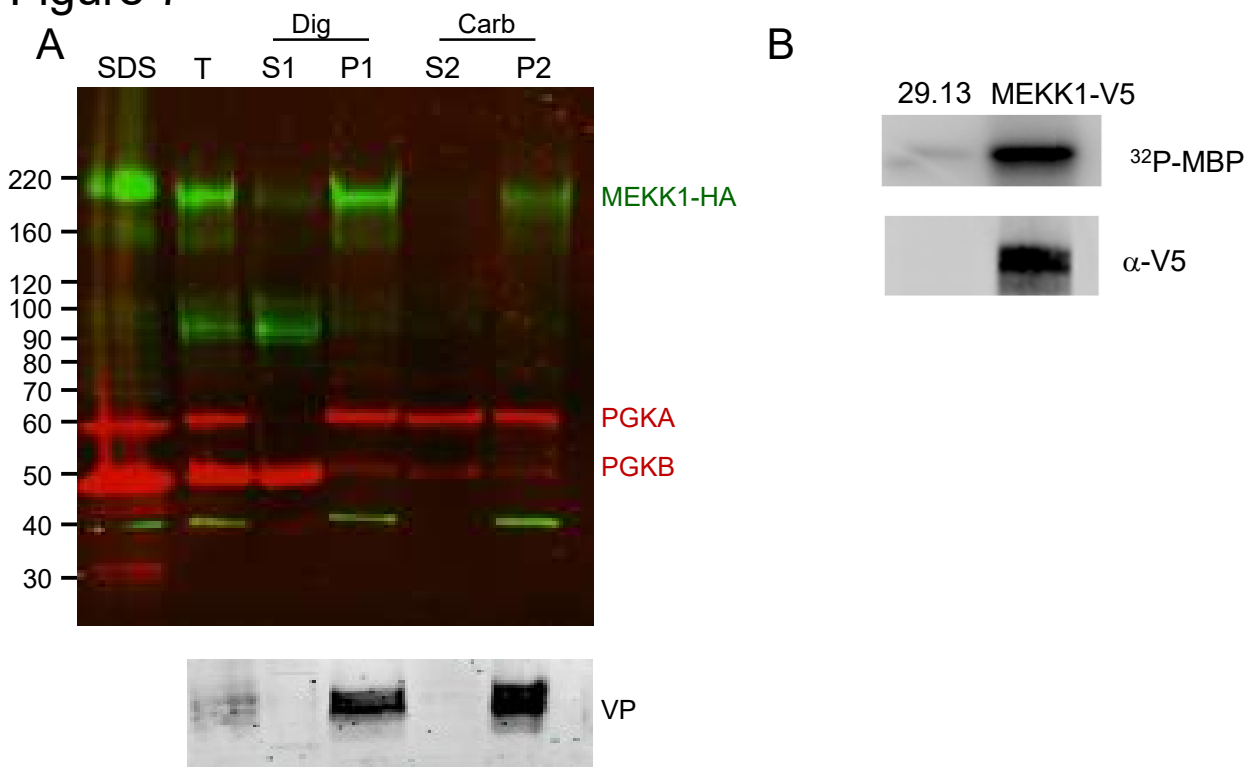

Figure 7. MEKK1 is an integral membrane protein which has protein kinase activity.
A) Cell fractionation. PF cells expressing MEKK1-HA were fractionated by digitonin treatment followed by carbonate extraction. After separation by SDS-PAGE and blotting, the blots were probed with mouse anti-HA (green) and rabbit anti-phosphoglycerate kinase (red) which detects the 56 kDa glycosomal form (PGKA) and the 47 kDa cytosolic isoform (PGKB). A parallel blot was also incubated with antibody to the acidocalcisome membrane protein vacuolar phosphatase (VP). SDS, SDS lysate; T, total after incubation with digitonin; S1, digitonin supernatant; P1, digitonin pellet; S2, carbonate supernatant; P2, carbonate pellet. Lanes contain fractions from 3×106cells.
B) Kinase activity. Immunoprecipitated MEKK1 from PF was incubated with γ 32P-ATP and the exogenous substrate myelin basic protein (MBP), followed by SDS-PAGE and transfer to nitrocellulose. A control immunoprecipitation used the untransfected parental line (29.13). Top: phosphorimaging demonstrates phosphorylation of MBP. Bottom: the blot was probed with anti-V5 mAb demonstrating the pulldown of the tagged protein.

Figure 8

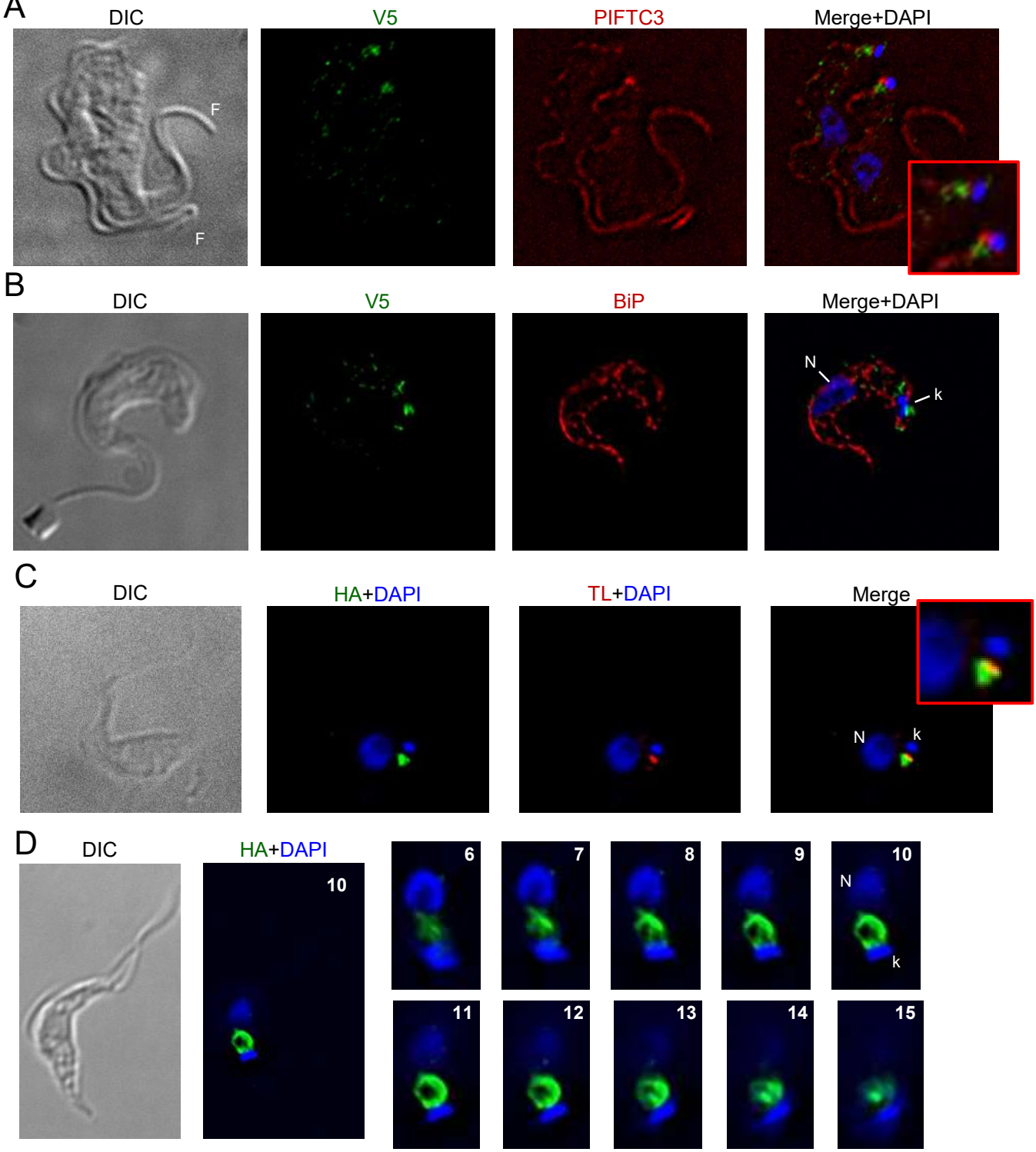

Figure 8. Predominant localization of epitope- tagged FHK near the kinetoplast. A, B) BF expressing FHK-V5 and co-stained with DAPI, anti-V5 antibodies, and either anti-PIFTC3 (A) or anti-BiP (B). Enlargement shows region around kDNA. The cell in (A) has duplicated both its nucleus (N) and kDNA (k) and is undergoing cytokinesis as evidenced by the presence of two flagella (F). The cell in panel B has an elongated, slightly V-shaped kinetoplast, indicating it is undergoing kinetoplast division and is in nuclear S phase. Note that a point of FHK-staining occurs at either pole of the elongated kDNA. **C)** PF expressing FHK-HA were incubated with biotinylated-tomato lectin (TL) at 4o and fixed prior to staining with DAPI, avidin and anti-HA. Enlargement shows region around kDNA. **D)** Whole cell and enlarged serial planes (numbered) of a DAPI-stained PF cell expressing FHK-HA. All images (except enlargements) are at the same magnification. Bar = 5 µm.

Figure 9

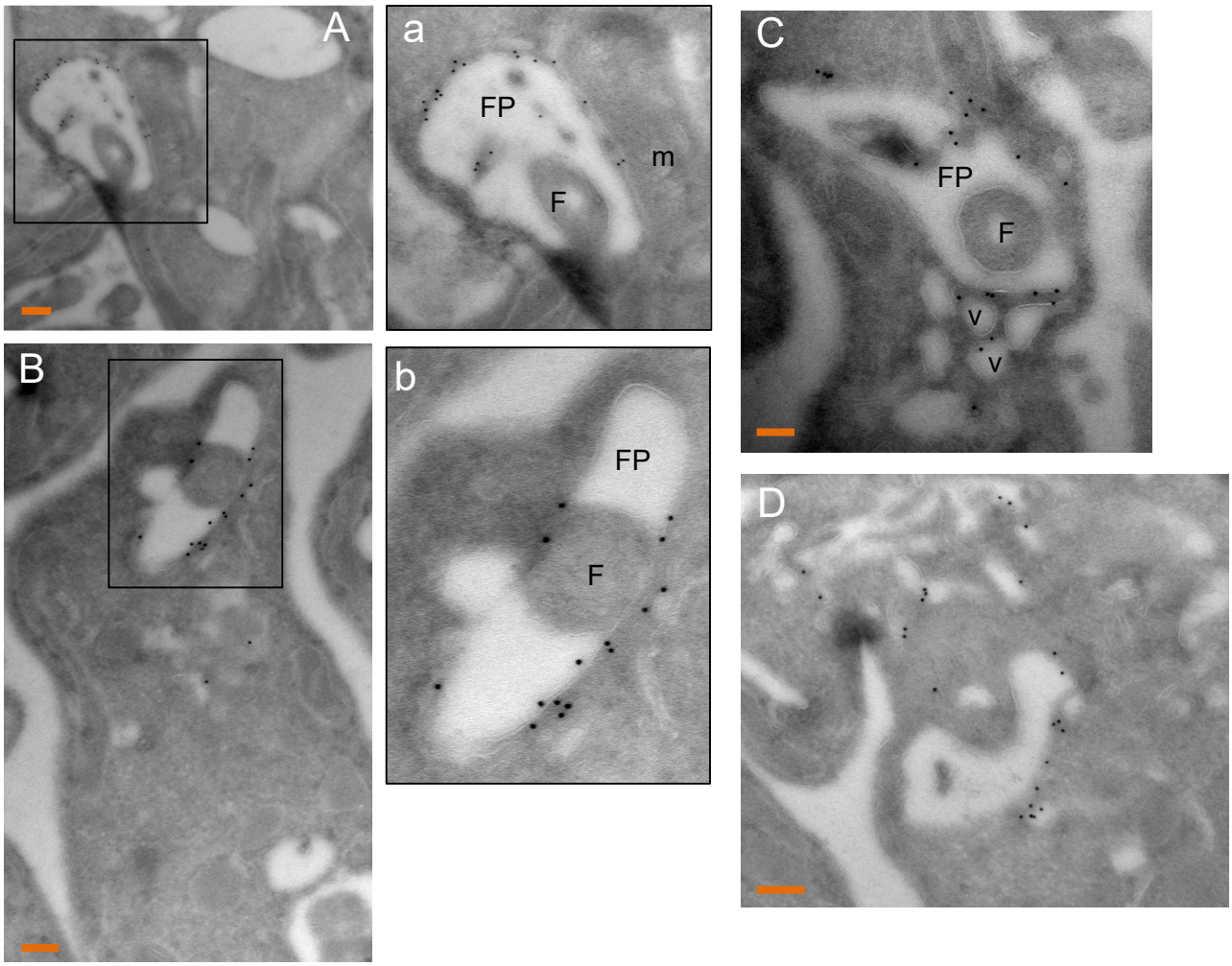

Fig. 9. Localization of FHK-HA to the flagellar pocket by immunoelectron microscopy
Procyclic form parasites expressing FHK C-terminally tagged with HA epitopes were stained with anti-HA revealed by protein-A gold 10 nm particles. A) The gold staining is on the flagellar pocket (FP) membrane but absent from the flagellum (F) and mitochondrion (m). Enlargement of the marked region is shown in panel a. B) Staining is predominantly at the flagellar pocket, and often one side shows more abundant FHK. Enlargement of the marked region is shown in panel b. C) The staining is sometimes seen on vesicles close to the FP. D) Occasional parasites showed staining outside the flagellar pocket. Bars, 100 nm.

Figure 10

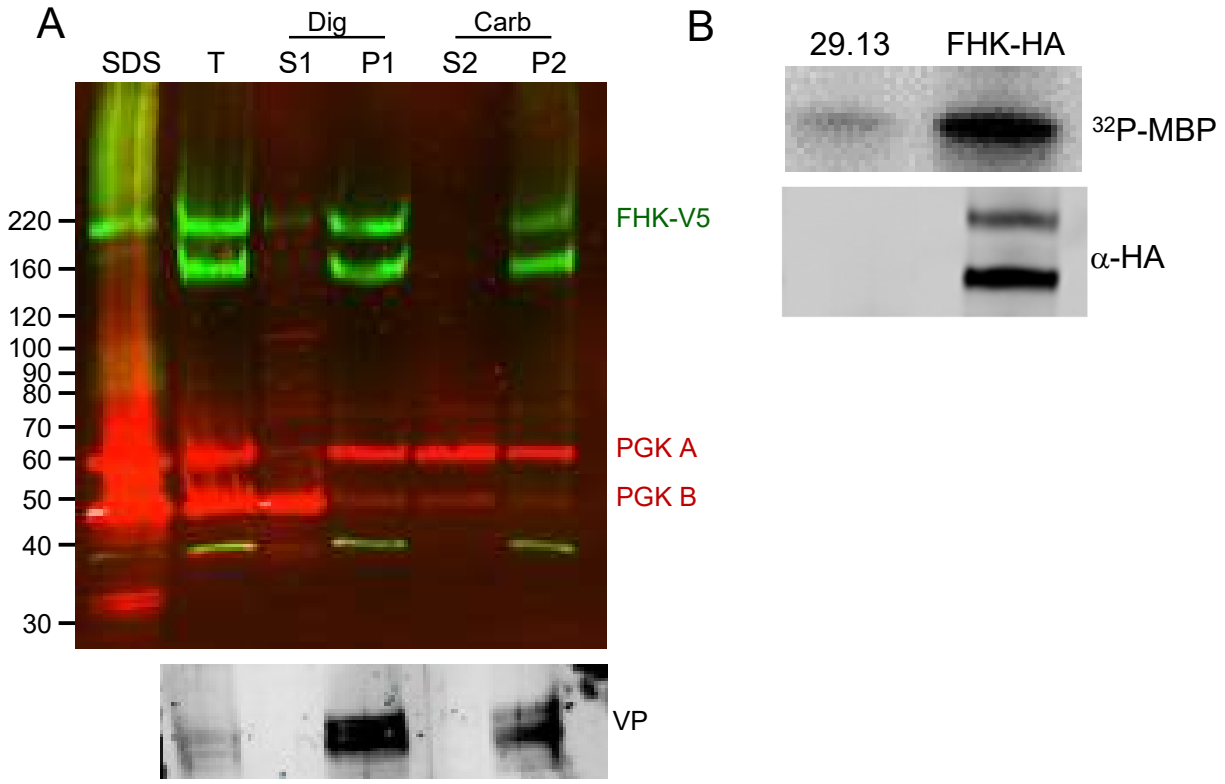

Figure 10. FHK is an integral membrane protein with protein kinase activity.
A) Cell fractionation and immunoblotting were as described in Fig. 7. **B)** Kinase activity as described in Fig. 9. FHK-HA was immunoprecipitated from PF and incubated with γ 32P-ATP and MBP. A negative control immunoprecipitation was performed using the untransfected parental line 29.13. Top: phosphorimaging demonstrates phosphorylation of MBP. Bottom: the blot was probed with anti-HA mAb demonstrating the pulldown of the tagged protein.